

Excellence in Chemistry Research

**Announcing
our new
flagship journal**

- Gold Open Access
- Publishing charges waived
- Preprints welcome
- Edited by active scientists



Meet the Editors of *ChemistryEurope*



Luisa De Cola

Università degli Studi
di Milano Statale, Italy



Ive Hermans

University of
Wisconsin-Madison, USA



Ken Tanaka

Tokyo Institute of
Technology, Japan

Generation and Characterization of a Tetraradical Embedded in a Curved Cyclic Paraphenylenes Unit

Yuki Miyazawa,^[a] Zhe Wang,^[a] Sayaka Hatano,^[a] Ryukichi Takagi,^[a] Hideto Matsuoka,^{*[b]} Naoka Amamizou,^[c] Yasutaka Kitagawa,^{*[c]} Eiichi Kayahara,^[d] Shigeru Yamago,^[d] and Manabu Abe^{*[a]}

Abstract: Unique spin–spin (magnetic) interactions, ring-size effects on ground-state spin multiplicity, and in-plane aromaticity has been found in localized 1,3-diradicals embedded in curved benzene structures such as cycloparaphenylenes (CPP). In this study, we characterized the magnetic interactions in a tetraradical consisting of two localized 1,3-diradical units connected by *p*-quaterphenyl within a curved CPP skeleton by electron paramagnetic resonance (EPR) spectroscopy and quantum chemical calculations. Persistent triplet species with zero-field splitting parameters similar to

those of a triplet 1,3-diphenylcyclopentane-1,3-diyl diradical were observed by continuous wave (CW) or pulsed X-band EPR measurements. The quintet state derived from the ferromagnetic interaction between the two triplet diradical moieties was not detected at 20 K under glassy matrix conditions. At the B3LYP/6-31G(d) level of theory, the singlet state was lower in energy than the triplet and quintet states. These findings will aid in the development of open-shell species for material science application.

Introduction

In recent decades, open-shell molecules, such as radicals, have attracted much attention not only in fundamental research, but also in materials science applications.^[1] For example, open-shell singlet diradicals (so-called diradicaloids)^[2] with a small highest occupied molecular orbital (HOMO)–lowest unoccupied molecular orbital (LUMO) gap induced by the quinoidal form (Figure 1a) have been developed as nonlinear optical materials, functional dyes, and imaging materials that respond to near-

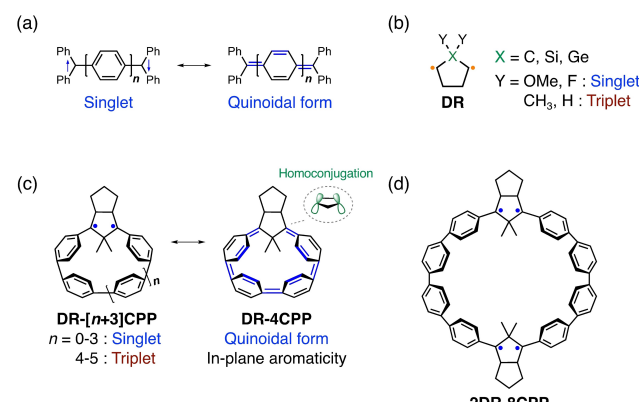


Figure 1. (a) Formation of quinoidal structure. (b) Substituent effects on the ground-state spin multiplicity of cyclopentane-1,3-diradical (DR). (c) Ring-size effects of cyclopentane-1,3-diradicals embedded in cycloparaphenylenes (CPP) on ground-state spin-multiplicity and in-plane aromaticity. (d) Tetraradical investigated in this study.

[a] Y. Miyazawa, Dr. Z. Wang, Dr. S. Hatano, Dr. R. Takagi, Prof. Dr. M. Abe
Department of Chemistry
Graduate School of Advanced Science and Engineering
Hiroshima University
1-3-1 Kagamiyama, Higashi-Hiroshima, Hiroshima 739-8526 (Japan)
E-mail: mabe@hiroshima-u.ac.jp
Homepage: <http://www.hiu-roc.com/>

[b] Prof. Dr. H. Matsuoka
Graduate School of Science
Osaka Metropolitan University
1-2-7-601, Asahimachi, Osaka 545-0051 (Japan)
E-mail: matsuoka.hideto@k.hokkyodai.ac.jp
Homepage: <https://h-matsuoka-lab.jp/>

[c] N. Amamizou, Prof. Dr. Y. Kitagawa
Graduate School of Engineering Science
Osaka University
1-3 Machikaneyama, Toyonaka, Osaka 560-8531 (Japan)
E-mail: kitagawa@cheng.es.osaka-u.ac.jp
Homepage: <https://rd.iai.osaka-u.ac.jp/en/d647465260622c64.html>

[d] Dr. E. Kayahara, Prof. Dr. S. Yamago
Institute for Chemical Research
Kyoto University
Uji, Kyoto 611-0011 (Japan)

Supporting information for this article is available on the WWW under <https://doi.org/10.1002/chem.202301009>

by homoconjugation at the bent cyclopentane-1,3-diradical unit (Figure 1c).

In this study, we designed and generated tetraradical **2DR-8CPP** with two localized 1,3-diradicals at remote positions within a curved CPP skeleton (Figure 1d) to understand the spin–spin (magnetic) interactions and characterize the open-shell species by electron paramagnetic resonance (EPR) spectroscopy and quantum chemical calculations. Fundamental knowledge of spin–spin interaction is indispensable for future materials science applications, such as soft magnets.

Results and Discussion

Synthesis of **2AZ-8CPP**

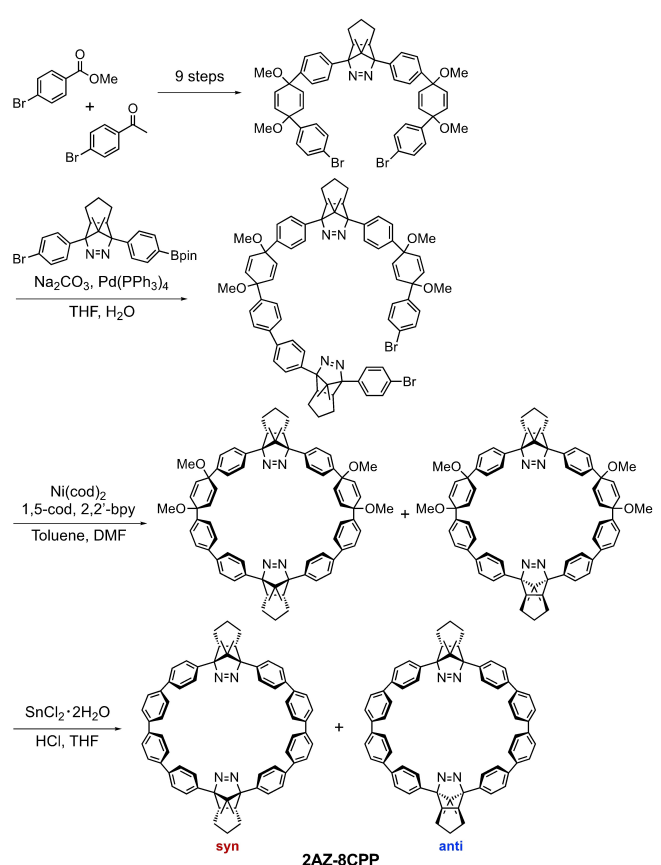
Tetraradical **2DR-8CPP** was generated by the photodenuitrogenation of bis-azo compound **2AZ-8CPP**. The azoalkane precursor was synthesized in 12 steps using 4'-bromoacetophenone and methyl 4-bromobenzoate as starting materials (Scheme 1).

Intramolecular Yamamoto coupling of the dibromide followed by reductive aromatization^[9] afforded syn- and anti-**2AZ-8CPP** in a total chemical yield of 0.03%. In the ¹H NMR (700 MHz) and ¹³C NMR (176 MHz) spectra, CH₃ signals were observed at δ_H=0.215, 0.221, and -1.19 (two overlapping signals) ppm and δ_C=17.06, 17.13, 17.42, 17.48 ppm, confirming

the presence of two isomers (Figure 2a). Density functional theory (DFT) calculations at the RB3LYP/6-311+G(2d,p) level^[10] predicted the ¹³C NMR chemical shifts of the four methyl carbons to be located at 18.48/19.01 and 18.54/18.81 ppm for the syn and anti isomers, respectively, which are in good agreement with the experimentally observed values. The higher field resonance of the CH₃ groups in the syn conformer than those in the anti conformer was also found in the computations. Based on the integral ratio of the ¹H NMR signals, the syn:anti isomer ratio was approximately 2:1. Single crystals of anti-**2AZ-8CPP** were coincidentally obtained from the precipitate during the gradual evaporation of a mixture of tetrahydrofuran (THF), dioxane, and a small amount of cyclohexane and analyzed by X-ray crystallography (Figure 2b). Although the solvent molecule cyclohexane was disordered, the strained structure of the anti conformer was confirmed by the X-ray crystallographic analysis. The bond lengths, average torsion angle ($\theta=23.1^\circ$), and bend angle of the benzene rings ($\alpha=12.3^\circ$) of the *p*-quaterphenylene units of anti-**2AZ-8CPP** are summarized in Figure 2b.

Photophysical property of **2AZ-8CPP**

The absorption and emission spectra of **2AZ-8CPP** in benzene solution are shown in Figure 3. A broad absorption maximum at approximately 327 nm ($\epsilon=6.0 \times 10^4 \text{ M}^{-1} \text{ cm}^{-1}$) was observed in the UV-visible absorption spectrum. Time-dependent DFT calculations^[11] at the B3LYP/6-311G+(2d,p) level revealed that the absorption was due to (HOMO – 1) – LUMO and HOMO –



Scheme 1. Synthesis of syn- and anti-**2AZ-8CPP**.

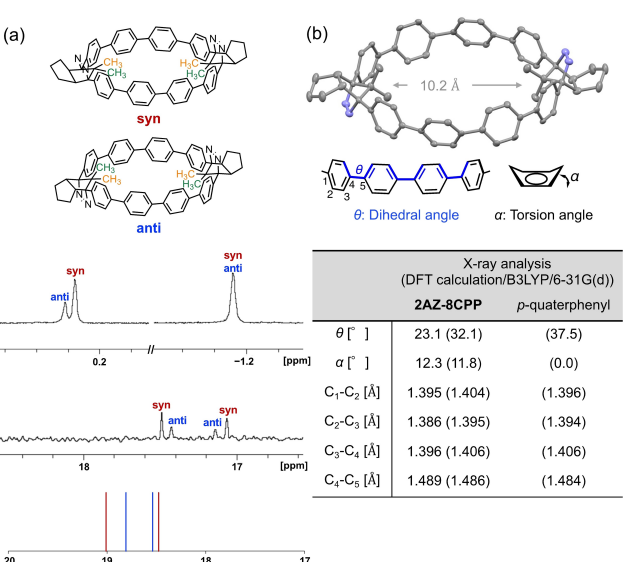


Figure 2. (a) ¹H NMR (700 MHz) (upper, H chemical shift of methyl groups: syn, -1.19 and 0.215 ppm; anti, -1.19 and 0.221 ppm) and ¹³C NMR (176 MHz) (middle, C chemical shift of methyl groups: syn, 17.06 and 17.48 ppm; anti, 17.14 and 17.42 ppm) spectra in CDCl₃ and chemical shifts of methyl carbons calculated at the B3LYP/6-311+G(2d,p) level (lower, C chemical shift of methyl groups: syn (red), 18.48 and 19.01 ppm; anti (blue), 18.54 and 18.81 ppm). (b) X-ray structure of **2AZ-8CPP** with thermal ellipsoids at 50% probability (gray, carbon; blue, nitrogen). Hydrogen atoms and solvent molecules are omitted for clarity.

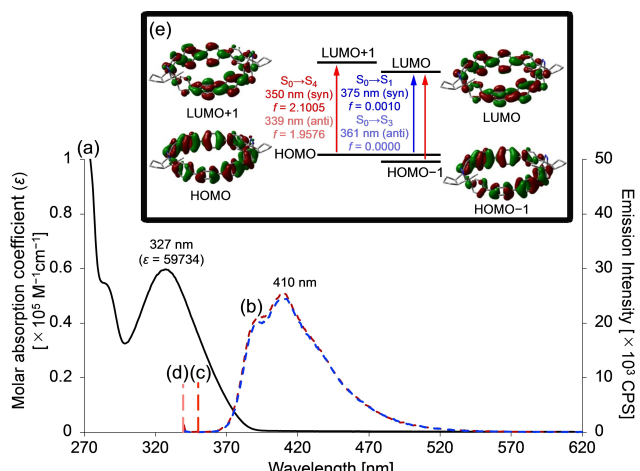


Figure 3. Absorption and emission analyses of **2AZ-8CPP** in benzene. (a) UV–visible absorption spectrum. (b) Emission spectrum at 330-nm excitation ($\text{Abs}_{330}=0.1$) under N_2 atmosphere (red) and air (blue) in benzene solution. $S_0\rightarrow S_4$ transition of the (c) syn and (d) anti isomers calculated by time-dependent density functional theory at the B3LYP/6-311G+(2d,p) level. (e) Kohn–Sham orbitals of the syn isomer.

(LUMO + 1) transitions ($S_0\rightarrow S_4$) with high oscillator strengths of $f=2.1005$ (syn) and 1.9576 (anti). The HOMO–LUMO transition ($S_0\rightarrow S_1$, syn; $S_0\rightarrow S_3$, anti) was forbidden because of the conserved symmetry. Normally, the weak $n-\pi^*$ transition ($\varepsilon \approx 100 \text{ M}^{-1}\text{cm}^{-1}$) of the azo chromophore should be observed at approximately 360 nm. However, it was hidden behind the strong absorption band from the π -conjugated system.

Weakly structured fluorescence was observed upon 330-nm excitation under both air and nitrogen atmosphere, and the emission intensity decreased slightly under air. The energy of the S_1 state calculated from the intersection of the absorption and emission spectra was 76 kcal mol $^{-1}$. The lifetimes of the fluorescence at 410 nm and 295 K, determined by the time-correlated single-photon counting method, were $\tau_f=1.2$ ns under N_2 and 1.1 ns under air. Relatively moderate fluorescence quantum yields of $\Phi_f=39\pm 1\%$ and $34\pm 1\%$ were obtained under N_2 and air, respectively. The phosphorescence of **2AZ-8CPP** in a 2-methyltetrahydrofuran (2-MTHF) matrix was not observed, even at 77 K under argon atmosphere. The relative energies of the T_1 state from S_0 state calculated at the UM06-2x/6-31G(d) level^[12] were 58.6 (syn) and 59.0 (anti) kcal mol $^{-1}$. This level of theory has reproduced well the experimental values of triplet excited-state molecules.^[13] Thus, the estimated energy differences between the S_1 and T_1 states (ΔE_{ST}) were 17.4 (syn) and 17.0 (anti) kcal mol $^{-1}$. These energies are smaller than that of the singlet state of molecular oxygen (${}^1\Delta_g=22.5$ kcal mol $^{-1}$), suggesting that the slight quenching of the fluorescence under air was that of the S_1 state by triplet oxygen.^[14]

The sub-microsecond and sub-nanosecond transient absorption (TA) of **2AZ-8CPP** upon 355-nm excitation at 295 K in benzene were measured by laser flash photolysis (LFP)^[15] and the randomly interleaved pulse train (RIPT) method,^[16] respectively (Figure 4). Transient species with broad absorption at approximately 560 nm [$k_d=(3.2\pm 1)\times 10^4 \text{ s}^{-1}$, $\tau=31\pm 1 \mu\text{s}$]

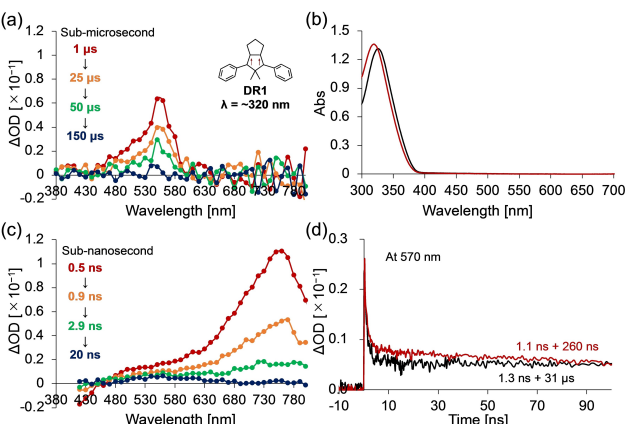


Figure 4. Time-resolved transient absorption (TA) spectra during the photolysis of **2AZ-8CPP** in benzene. (a) Sub-microsecond time-resolved TA spectra in benzene under N_2 atmosphere at 295 K. (b) Ground state UV–visible absorption spectra before (black) and after (red) the sub-microsecond laser flash photolysis measurements under N_2 atmosphere. (c) Sub-nanosecond time-resolved TA spectra in benzene under Ar atmosphere at 295 K. (d) Time profiles at 570 nm obtained by sub-nanosecond time-resolved spectroscopic analysis under Ar atmosphere (black) and air (red).

were observed in the sub-microsecond TA analysis under N_2 atmosphere (Figure 4a). The absorption of the transient species at approximately 560 nm was significantly quenched under air [$k_d=(3.8\pm 1)\times 10^6 \text{ s}^{-1}$, $\tau=260\pm 5 \text{ ns}$], suggesting that it originated from the triplet species. A small change in the UV–visible absorption spectra of the ground-state sample before and after the sub-microsecond LFP measurements was observed (Figure 4b). To obtain information about the photoproducts, the photolysate was analyzed by high-resolution (HR) mass spectrometry (*p*-ESI/MeOH),^[17] which confirmed the formation of compounds upon N_2 elimination (see below). The electronic absorption of triplet 1,3-diphenylcyclopentane-1,3-diyli diradical DR1 was reported to appear at approximately 320–350 nm.^[18] Thus, the transient species observed at approximately 560 nm in this study was assigned not to the triplet state of the diradical, but to the triplet excited state of the π -conjugated paraphenylen moiety of **2AZ-8CPP**. Sub-nanosecond TA analysis was also performed to examine the more short-lived species (Figure 4c). A transient species with a strong absorption maximum at ~ 750 nm was observed and assigned to the $S_1\rightarrow S_n$ transition. Its absorption was not quenched under air (Figure 4d), and its lifetime (under Ar, $\tau=1.3$ ns; under air, $\tau=1.1$ ns) was nearly consistent with the fluorescence lifetime. Both the excited singlet and triplet states were simultaneously observed at a wavelength of 570 nm (Figure 4d). Interestingly, the intensity of the triplet TA under air was higher than that under Ar atmosphere. Intersystem crossing from the S_1 to the T_1 state was accelerated in the presence of ${}^3\text{O}_2$.

Photolysis of **2AZ-8CPP** in solution at room temperature

The photoreaction of a mixture of syn- and anti-**2AZ-8CPP** (0.9 mM) using 365-nm LED light at 296 K in a degassed C_6D_6

solution in a sealed NMR tube under vacuum was monitored by ^1H NMR (400 MHz) spectroscopy (Figure 5). During the irradiation of **2AZ-8CPP**, singlet signals corresponding to the CH_3 groups originating from the photoreaction products were observed at the high magnetic field region (-1.37 , 0.70 , and 0.94 ppm in orange color) with the concomitant decrease of the signals of the CH_3 groups in **2AZ-8CPP** (-0.77 and 0.36 ppm in green color). The new signal at -1.37 ppm gradually decreased, while the signals at the low magnetic field region (0.00 , 0.04 , and 0.90 ppm in blue color) gradually increased. Furthermore, the three signals broadened as light irradiation was continued, indicating that secondary photoreaction of the primary products occurred to give a mixture of products (see Supporting Information (SI)). As identifying the products by NMR analysis was difficult, the photolysate was analyzed by HR mass spectrometry (*p*-ESI/MeOH) after unsealing the NMR tube. The presence of products with $\text{C}_{68}\text{H}_{60}$ was confirmed, suggesting that double denitrogenation (-2N_2) of **2AZ-8CPP** occurred under photolysis conditions. In addition to the denitrogenated products, oxygenated compound $\text{C}_{68}\text{H}_{60}\text{O}_4$ was observed in the photolysate. Similar oxygenated compounds were also found in the product analysis of **DR-6CPP**,^[8] suggesting that the photo-products of **2AZ-8CPP** were O_2 reactive.

Photolysis of **2AZ-8CPP** under low-temperature matrix conditions

To directly observe **2DR-8CPP**, the photolysis of **2AZ-8CPP** ($100 \mu\text{M}$) in a 2-MTHF matrix in a sealed quartz tube under vacuum was monitored by EPR spectroscopy. After 1 h of irradiation with a UV lamp ($\lambda_{\text{em}} > 250 \text{ nm}$) at 20 K , EPR signals with zero-field splitting (zfs) parameters of $|D/\text{hc}| = 0.045 \text{ cm}^{-1}$ and $|E/\text{hc}| \leq 0.001 \text{ cm}^{-1}$ were observed (Figure 6a). These values are slightly smaller than those reported for triplet 1,3-diphenylcyclopentane-1,3-diyl diradical **DR1** ($|D/\text{hc}| = 0.050 \text{ cm}^{-1}$ and $|E/\text{hc}| \leq 0.001 \text{ cm}^{-1}$).^[19]

The quintet state of the tetraradical with a smaller D value ($|D/\text{hc}| = 0.012$ (syn) and 0.014 (anti) cm^{-1} , computed at the (RO)BP/EPR-II/B3LYP/6-31G(d)^[20] level of theory using ORCA 4.2.1^[21]) was not detected after further photolysis at the same

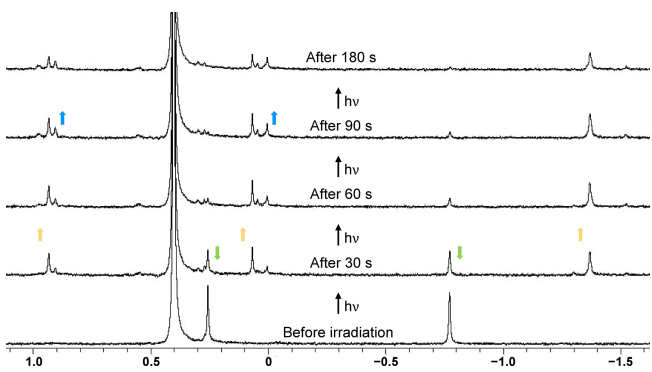


Figure 5. ^1H NMR analysis (400 MHz) of the photolysis of **2AZ-8CPP** (0.9 mM) using 365-nm LED light in degassed C_6D_6 solution.

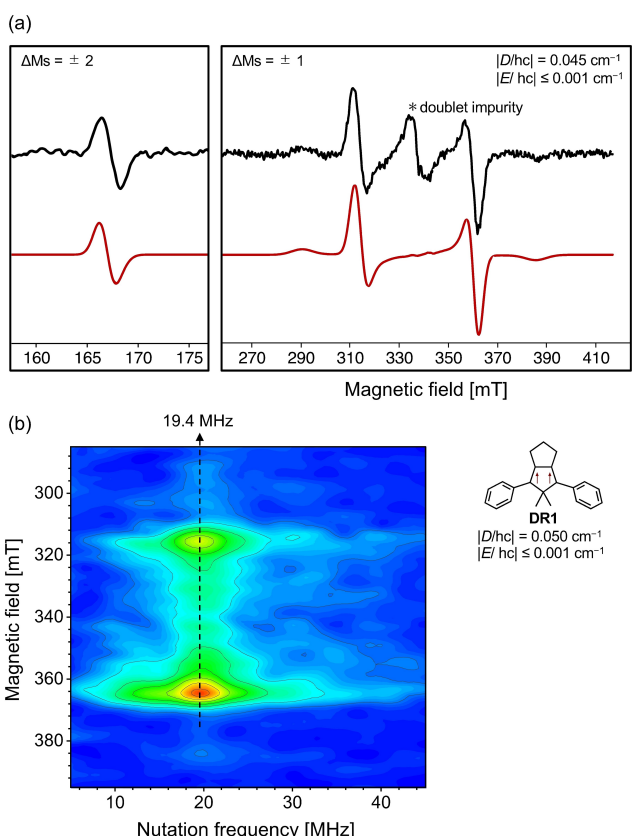


Figure 6. (a) EPR spectrum at 20 K (black) after photolysis of **2AZ-8CPP** in a 2-methyltetrahydrofuran matrix ($100 \mu\text{M}$) using UV light under vacuum and simulated EPR spectrum (red). The zero-field splitting parameters of the EPR signals are $|D/\text{hc}| = 0.045 \text{ cm}^{-1}$ and $|E/\text{hc}| \leq 0.001 \text{ cm}^{-1}$ and $|D/\text{hc}| = 0.050 \text{ cm}^{-1}$ and $|E/\text{hc}| \leq 0.001 \text{ cm}^{-1}$ for **DR1**. (b) 2D pulsed EPR signal at 20 K after photolysis for 10 h in a toluene matrix (0.1 mM) using UV light under vacuum.

temperature. The ratio of the intensity of the half-field transition to that of the allowed transition was much stronger than that observed in typical triplet species, which could not be reproduced by a common line-shape model based on a convolution of Gaussian and Lorentzian functions. For $S \geq 1$ spin systems, line broadening is often explained by considering the distributions of D and E originating from local structural heterogeneities ('strain').^[22] The unusual intensity ratio was reproduced well (red-colored one in Figure 6a) using a phenomenological D -strain model because the half-field resonance position was dominated by the g values. Because the macrocyclic compound had a rigid structure, the structural distribution was due to being frozen under the EPR measurement conditions before the most stable structure was taken.

To determine the spin state of the multiradical, 2D pulsed EPR measurements^[23] were conducted in a toluene matrix ($100 \mu\text{M}$) under vacuum. In this method, the spin state of the multiradical can be determined from the ratio of the nutation frequencies ω_n of the peaks in the 2D pulsed EPR spectra [Eq. (1)]:

$$\omega_n = [S(S+1) - M_s(M_s-1)]^{1/2} \omega_1 \quad (1)$$

where S is the spin quantum number and M_s is the magnetic moment. The measurements were conducted after UV irradiation at 20 K for 10 h. A triplet species with a nutation frequency of 19.4 MHz was observed (triplet state $\sqrt{2} \omega_1$, Figure 6b). The EPR signal at approximately 330 mT originated from a doublet species with a nutation frequency of $\omega_1 = 14$ MHz (SI). A high-spin state, such as a quintet state with a large nutation frequency, was not observed after the long period of photolysis, suggesting that only triplet species existed as a detectable paramagnetic species under the measurement conditions.

Quantum chemical calculations on 2DR-8CPP

Finally, the quintet, triplet, and singlet states of **2DR-8CPP** were computed at the B3LYP/6-31G(d) level^[24] using the Gaussian 09 rev. D01 program (Figure 7). For the singlet state, not only the closed-shell state, but also the open-shell state with a broken-symmetry (BS) structure was considered. As shown in Figure 7, for **2DR-8CPP** containing two diradical units, the combination of ferromagnetic and antiferromagnetic coupling between the intra- and intermolecular interactions should be considered. Two alignments in the singlet state, “intramolecular-ferromagnetic/intermolecular-antiferromagnetic” and “intramolecular-antiferromagnetic/intermolecular-antiferromagnetic” were constructed and denoted as BS-singlet state 1 and BS-singlet state 2, respectively. Because the triplet state could not be represented by a single determinant and thus necessitated a multireference calculation method, we focused on the quintet and singlet states in the spin-unrestricted DFT calculations.

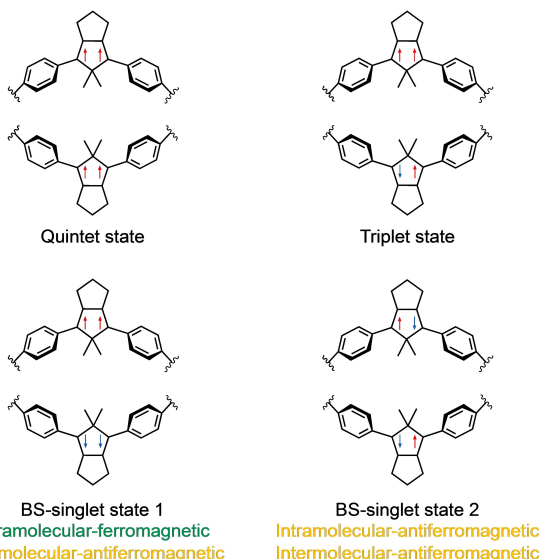


Figure 7. Illustrations of spin alignments in the quintet, triplet, and broken symmetry (BS)-singlet states.

The orbital-averaged spin coupling parameter (J) was obtained from the calculated energies by applying the Ising Hamiltonian, and the energy gap between the singlet and triplet states (S-T gap: $2J$) was then estimated (SI). All calculations were conducted in both gas phase and THF solution.

First, the structure of each spin state was optimized (SI). The optimized structures in THF solution (Figure 8a) were almost the same as those in the gas phase. A nearly circular structure was observed in the closed-shell singlet state, whereas an elliptical structure was formed in the quintet state. This was due to the loss of planarity upon formation of an open-shell structure at the diradical unit. On the other hand, the quintet and BS-singlet states were not significantly different, indicating that the open-shell character of the diradical unit largely contributed to the ring skeleton. The spin density distributions of the quintet, BS-singlet 1, and BS-singlet 2 states, calculated using the optimized structures, are shown in Figure 8b. In all models, the spin density was located mainly in the diradical unit and phenyl rings on both sides. The spin densities in the diradical units were ferromagnetic in the quintet and BS-singlet 1 states and antiferromagnetic in the BS-singlet 2 state, although their distributions were almost the same.

The ground-state spin multiplicity was estimated by comparing the total energies of the optimized structures. The relative energies of the closed- and open-shell singlet states to that of the quintet state are summarized in Table 1. Both BS-singlet states were slightly more stable than the quintet state.

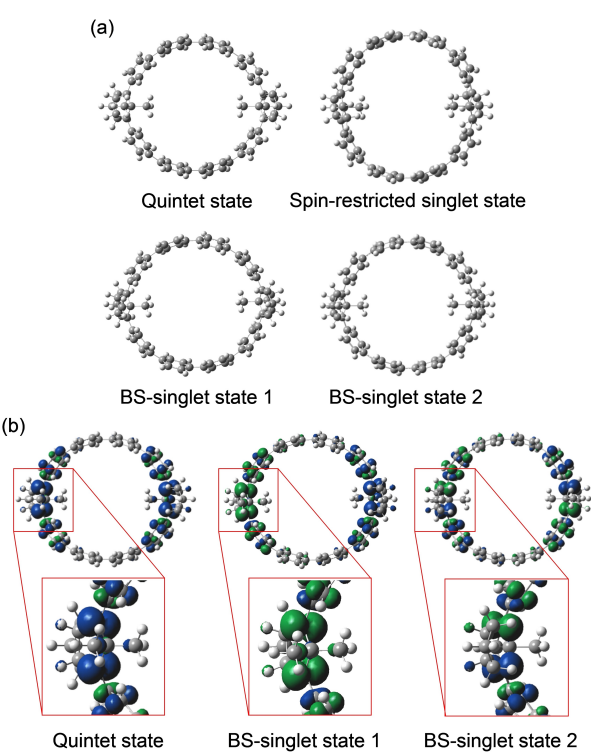


Figure 8. (a) Optimized structures of the quintet, closed-shell (spin-restricted) singlet, and open-shell singlet (broken-symmetry (BS)-singlet 1 and 2) states. (b) Calculated spin density distributions (isovalue = 0.005). The up and down spin density distributions are shown in blue and green, respectively.

Table 1. Energies of the optimized singlet states relative to that of the quintet state in THF solvent.

	Quintet	Spin states		
		BS-singlet 1	BS-singlet 2	Closed-shell
Relative Energy [kcal mol ⁻¹] ^[a]	0.00 (0.00)	-0.39(-0.35) [-0.61]	-0.14 (-0.13) [-0.22]	+24.9 (+25.7)

[a] Gas-phase values are also provided in parenthesis. Approximate spin-projected values for BS-singlet states are provided in square brackets.

indicating that the ground state of **2DR-8CPP** is a singlet. The closed-shell singlet state became unstable above 20 kcal mol⁻¹, indicating the significant effect of static electron correlation. Moreover, the energy of BS-singlet state 1 was lower than that of BS-singlet state 2 by 0.25 kcal mol⁻¹. The theoretical calculations were performed in both the gas phase and THF solution, although no difference in relative stability due to the difference in chemical environment was observed.

Spin contamination error was included in the BS solution for the open-shell singlet states. To remove this error, one diradical unit in BS-singlet state 1 was regarded as spin S=1, and the spin projection method was applied for the magnetic interaction between the diradical units by assuming a two-spin Heisenberg model.^[25] The relative energies of BS-singlet states 1 and 2 upon removal of spin contamination using the Yamaguchi equation^[26] (SI) were -0.61 and -0.22 kcal mol⁻¹, respectively. This result indicates that spin contamination error in the energy cannot be ignored. The energy of BS-singlet state 2 was also expected to contain spin contamination error. However, the spin projection method cannot be applied because the two-site Heisenberg model is not strictly applicable to this state. The energy excluding the spin contamination error was estimated to be stable at 0.08 kcal mol⁻¹ if the magnetic interaction between the two diradical units was negligible (SI). Because spin contamination sometimes strongly affects even the optimized structure of an open-shell singlet,^[27] we also determined its effect by applying the approximate spin-projected optimization method.^[26b] The optimized structure of BS-singlet state 1 was almost the same as that before using the spin projection method, and the relative energy remained unchanged at -0.61 kcal mol⁻¹. On the other hand, the structure of BS-singlet state 2 changed very slightly, and the relative energy changed to -0.23 kcal mol⁻¹. Because the magnetic interaction between the two diradical units is presumably negligible in BS-singlet state 2, it is difficult to discuss this in detail. However, the structures of the quintet and BS-singlet 1 states are almost identical, whereas that of the BS-singlet 2 state is slightly different. In other words, the spin interactions in the diradical units of the quintet and BS-singlet 1 states are ferromagnetic, whereas that of the BS-singlet 2 state is antiferromagnetic, suggesting that the degree of curvature of the diradical unit is slightly different between the ferromagnetic and antiferromagnetic coupling states.

Finally, we estimated the magnetic interactions in the diradical unit (J_{intra}) and between the diradical units (J_{inter}). J_{inter} was antiferromagnetic (-0.21 kcal mol⁻¹), whereas J_{intra} was

ferromagnetic (+0.16 kcal mol⁻¹) in THF solution. The quintet, triplet, and singlet energy levels estimated from the J values are shown in Figure 9. The open-singlet state was more stable than the triplet (-0.37 kcal mol⁻¹) and quintet (-0.41 kcal mol⁻¹) states.

Variable temperature (VT)-EPR measurements during photolysis of **2AZ-8CPP** under low-temperature matrix conditions

To obtain more information about the multiradicals generated during the photolysis of **2AZ-8CPP**, VT-EPR measurements were conducted (Figure 10). After 2 h of photolysis at 5 K, a typical signal stemming from persistent triplet species was observed at the half-field region of ~166 mT.

The intensity measurements were conducted at a microwave power of 0.63 mW, for which signal saturation was not observed even at 5 K. As the temperature gradually increased, a decrease in the EPR signal intensity at 166 mT was observed (Figure 10a). A plot of the signal intensity I versus temperature T revealed that the IT values gradually decreased with decreasing temperature, indicating that the triplet state was thermally populated as an excited state (Figure 10b). As observed for **DR-6CPP**,^[8] the multiradicals in the macrocyclic skeleton were also thermally reactive, even at 40 K, resulting in a decrease in signal intensity above ~40 K. Thermal reactivity was confirmed by the fact that the EPR signal intensity at 5 K was not recovered after warming the EPR sample to 40 K. From the least-squares fit obtained by the Bleaney–Bowers analysis^[28] ($R^2 = 0.9814$, using points from 5 to 30 K), the singlet (E_S) and triplet (E_T) energy gap ΔE_{S-T} was determined to be -23 ± 1 kcal mol⁻¹, indicating that the ground state was a singlet. This

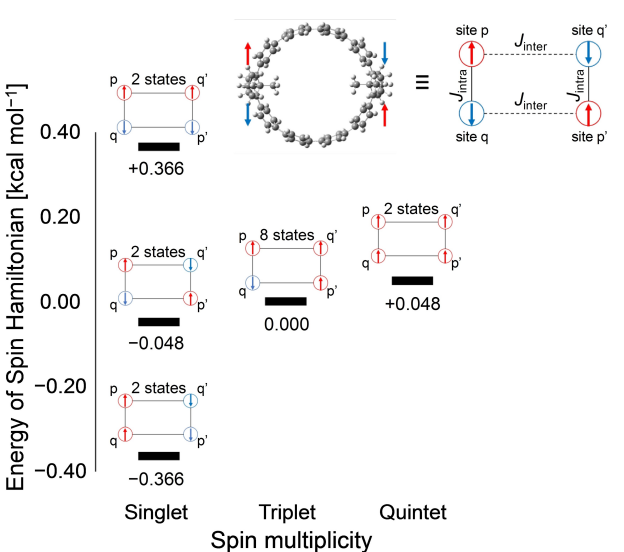


Figure 9. Energy diagram based on the calculated intra- ($J_{\text{intra}} = +0.16$ kcal mol⁻¹) and intermolecular ($J_{\text{inter}} = -0.21$ kcal mol⁻¹) magnetic interactions. The total number of states in each spin multiplicity are also presented in the figure.

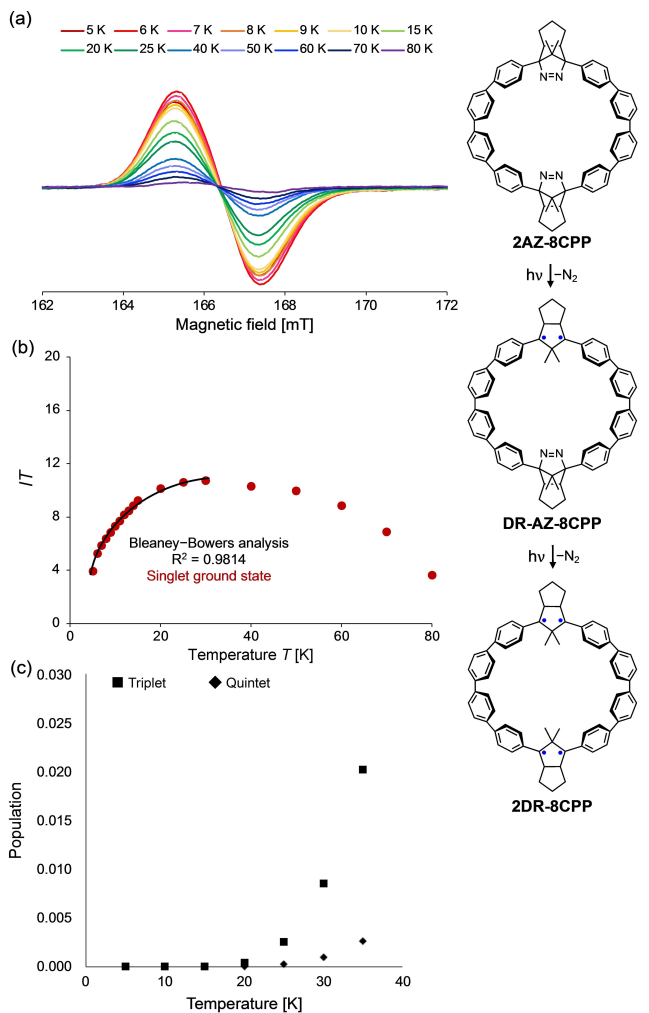


Figure 10. (a) Temperature dependence of the EPR signal intensity at the half-field region after photolysis of **2AZ-8CPP** using high pressure Hg light in a 2-methyltetrahydrofuran matrix (100 μ M) under vacuum. (b) Plot of the signal intensity I and temperature T and least-squares fit obtained by the Bleaney–Bowers analysis. (c) Simulated populations of the triplet and quintet states using the Boltzmann distribution.

value was smaller than the calculated ΔE_{S-T} energy gap in the tetraradical species (Figure 9).

During the photolysis of **2AZ-8CPP**, three paramagnetic species, namely the triplet states of **DR-AZ-8CPP** and **2DR-8CPP** and quintet state of **2DR-8CPP**, may be detected by the EPR measurements. Similarly, for **DR1**,^[19] the triplet ground state, formed by monodenitrogenation of **2AZ-8CPP**, was predicted for **DR-AZ-8CPP** (Figure 9). When **2DR-8CPP** was generated by a second denitrogenation reaction, the singlet state was expected to have a large population because it was computed to be the ground state. The EPR signal of the triplet state of **2DR-8CPP** might overlap with that of **DR-AZ-8CPP**. The experimentally determined small ΔE_{S-T} (Figure 10b) was due to the generation of a mixture of **DR-AZ-8CPP** having a triplet ground state and **2DR-8CPP** having a singlet ground state during the photolysis of **2AZ-8CPP**. Based on the computed energy gaps between the singlet, triplet, and quintet states of

tetraradical **2DR-8CPP**, the distribution of each spin state was determined (Figure 10c). The population of the quintet state was almost negligible at 20 K, although a small amount of the triplet state was present. Thus, detection of only the triplet state in the EPR analysis of **2DR-8CPP** is reasonable. The distribution of the quintet state could be augmented by increasing the temperature; however, the decomposition of multiradicals above 30 K hindered the observation of the quintet state.

Conclusion

In summary, a tetraradical embedded in a curved cycloparaphenylen (CPP) skeleton was generated and characterized for the first time to examine the reactivity and spin–spin (magnetic) interaction of the two diradical units in the bent molecular structure. The bis-azo compound **2AZ-8CPP**, the precursor of tetraradical **2DR-8CPP**, was successfully synthesized as two isomers with syn and anti configurations. The singlet and triplet excited states of the paraphenylen moiety of **2AZ-8CPP** were detected by transient absorption spectroscopy, and their reactivities were characterized at the sub-nanosecond and sub-microsecond time scales, respectively. Persistent triplet species were observed by the EPR measurements at 20 K during the photolysis of **2AZ-8CPP** under glassy matrix conditions. The quintet state of **2DR-8CPP** was not observed under the EPR measurement conditions because of its negligible population. Quantum chemical calculations of the spin–spin interaction in **2DR-8CPP** within the curved CPP skeleton revealed the open-shell character of the two diradical units in the macrocyclic structure. The magnetic interactions in the diradical unit (J_{intra}) and between the diradical units (J_{inter}) were ferromagnetic and antiferromagnetic, respectively. Thus, the open-shell singlet state of **2DR-8CPP** was slightly lower in energy than the corresponding triplet and quintet states. The theoretical prediction was confirmed by VT-EPR measurement during the photolysis of **2AZ-8CPP**.

Experimental Section

All synthetic procedures and characterization data (NMR, mass, UV-vis, IR, X-ray crystallography, fluorescence, EPR), and computation results are included in the Supporting Information.

The sub-microsecond transient absorption (TA) measurement of **2AZ-8CPP:** The sample solution was prepared for **2AZ-8CPP** (0.4 mg) was dissolved in C_6H_6 (10 mL). The sample solution was placed in a four-sided 1 cm quartz cuvette and N_2 bubbling was performed for 15 min. Transient absorption (TA) upon 355-nm excitation using a 355-nm yttrium aluminum garnet (YAG) laser (4 mJ/pulse, 4 ns pulse width) was measured at 295 K. The solution in the cuvette was refilled and the same measurement was conducted under air.

The sub-nanosecond transient absorption (TA) of **2AZ-8CPP:** The measurement solution was prepared for **2AZ-8CPP** (1 mg) was dissolved in C_6H_6 (5 mL). The sample solution was placed in a 0.2 cm quartz cuvette and Ar bubbling was performed for 15 min. Transient absorption (TA) upon 355-nm excitation using a 355-nm laser (10 μ J/pulse, 25 ps pulse width) was measured at 295 K. The

solution in the cuvette was refilled and the same measurement was conducted under air.

Photoreaction of 2AZ-8CPP: 2AZ-8CPP (0.4 mg) was dissolved in C₆D₆ (0.5 mL) and transferred to an NMR tube (diam. 5 mm). The NMR tube was sealed after freeze-pump thaw cycling (four times) using an oil diffusion pump. Photoreaction was conducted at 296 K using 365-nm LED light as a light source and ¹H NMR was measured as appropriate. The distance between LED light and sample tube was fixed at 7 cm.

Photolysis of 2AZ-8CPP under low-temperature matrix conditions: The sample solution of 2AZ-8CPP in 2-MTHF (100 μM) was transferred to a quartz tube and sealed under vacuum. Photoreaction was conducted at 20 K using UV light as a light source and monitored by EPR spectroscopy.

Deposition Number(s) 2259120 (for anti-2AZ-8CPP) contain(s) the supplementary crystallographic data for this paper. These data are provided free of charge by the joint Cambridge Crystallographic Data Centre and Fachinformationszentrum Karlsruhe Access Structures service.

Acknowledgements

This work was supported by JSPS KAKENHI Grant Number 22J10450. M.A. acknowledges financial support from JSPS KAKENHI (grant nos. JP17H03022, 20K21197, 21H01921, and 22K19033) and JST CREST (grant no. JPMJCR18R4). Mass spectrometry and single-crystal X-ray diffraction measurements were performed at the Natural Science Center for Basic Research and Development (N-BARD) of Hiroshima University. Y.K. acknowledges financial support from JSPS KAKENHI (grant nos. JP21H01951 and JP22H02050) and QIQB, ICS-OTRI, and ICS-SRN at Osaka University.

Conflict of Interests

The authors declare no conflict of interest.

Data Availability Statement

The data that support the findings of this study are available from the corresponding author upon reasonable request.

Keywords: Cycloparaphenylenes · in-plane conjugation · multiradical · spin interaction · spin multiplicity

- [1] a) M. Abe, *Chem. Rev.* **2013**, *113*, 7011–7088; b) L. Salem, C. Rowland, *Angew. Chem. Int. Ed.* **1972**, *11*, 92–111; c) Z. Zeng, X. Shi, C. Chi, J. T. L. Navarrete, J. Casado, J. Wu, *Chem. Soc. Rev.* **2015**, *44*, 6578–6596; d) T. Kubo, *Bull. Chem. Soc. Jpn.* **2021**, *94*, 2235–2244; e) A. Konishi, M. Yasuda, *Chem. Lett.* **2021**, *50*, 195–212; f) T. Taniguchi, *Chem. Soc. Rev.* **2021**, *50*, 8995–9021; g) Y. Tan, S.-N. Hsu, H. Tahir, L. Dou, B. M. Savoie, B. W. Boudouris, *J. Am. Chem.* **2022**, *144*, 626–647; h) S. Dong, Z. Li, *J. Mater. Chem. C* **2022**, *10*, 2431–2449; i) S. Kasemthaveechok, L. Abella, M. Jean, M. Cordier, N. Vanthuyne, T. Guizouarn, O. Cador, J. Autschbach, J. Crassous, L. Favreau, *J. Am. Chem. Soc.* **2022**, *144*, 7253–7263; j) X. Li, Y.-L. Wang, C. Chen, Y.-Y. Ren, Y.-F. Han, *Nat. Commun.* **2022**, *13*, 5367; k) Z. Wang, J. Zhou, Y. Zhang, W. Zhu, Y. Li, *Angew. Chem. Int. Ed.* **2022**, *61*, e202113653; l) C. Wang, H. Hao, K. Tajima, *Adv. Sci.* **2022**, *9*; m) S. Choppella, G. Paramasivam, S. Sambasivam, M. K. Ravva, *J. Electron. Mater.* **2022**, *52*, 1681–1690; n) Z. Yue, J. Liu, M. Baumgarten, D. Wang, *J. Phys. Chem. A* **2023**, *127*, 1565–1575; o) R. A. Shehzad, J. Iqbal, S. Ali, H. Anwar, *J. Mol. Graph.* **2023**, *121*; p) A. Abdurahman, J. Wang, Y. Zhao, P. Li, L. Shen, Q. Peng, *Angew. Chem. Int. Ed.* **2023**, *62*, e202300772; q) B. Hou, K. Li, H. He, J. Hu, Z. Xu, Q. Xiang, P. Wang, X. Chen, Z. Sun, *Angew. Chem. Int. Ed.* **2023**, *62*, e202301046.

- [2] a) M. Nakano, *Excitation Energies and Properties of Open-Shell Singlet Molecules*, Springer, Berlin, 2014; b) J. Wu, *Diradicaloids*, Jenny Stanford Publishing, New York, 2022; c) A. Konishi, M. Yasuda, *Advances in Physical Organic Chemistry* **2021**, *55*, 17–40; d) S. Kato, *Advances in Physical Organic Chemistry* **2021**, *55*, 41–66; e) F. Kuriakose, M. Commodore, C. Hu, C. J. Fabiano, D. Sen, R. R. Li, S. Bisht, Ö. Üngör, X. Lin, G. F. Strouse, E. A. Deprince, R. A. Lazenby, F.-V. Mentink, M. Shatruk, I. V. Alabugin, *J. Am. Chem. Soc.* **2022**, *144*, 23448–23464; f) X. Tian, J. Guo, W. Sun, L. Yuan, C. Dou, Y. Wang, *Chem. Eur. J.* **2022**, *28*; g) K. Li, Z. Feng, H. Ruan, Q. Sun, Y. Zhao, X. Wang, *Chem. Commun.* **2022**, *58*, 6457–6460; h) F. Wu, J. Ma, F. Lombardi, Y. Fu, F. Liu, Z. Huang, R. Liu, H. Komber, D. I. Alexandropoulos, E. Dmitrieva, T. G. Lohr, N. Israel, A. A. Popov, J. Liu, L. Bogani, X. Feng, *Angew. Chem. Int. Ed.* **2022**, *61*, e202202170; i) A. Maiti, B. J. Elvers, S. Bera, F. Lindl, I. Krummenacher, P. Ghosh, H. Braunschweig, C. B. Yıldız, C. Schulzke, A. Jana, *Chem. Eur. J.* **2022**, *28*, e202104567; j) S. Mori, S. Q. Moles, N. Tabaka, R. Kishi, R. N. González, A. Harbuzaru, R. O. Ponce, J.-B. Marín, S. Suzuki, C. Kitamura, C. J.-G. Gómez, Y. Dai, F. Negri, M. Nakano, S. Kato, J. Casado, *Angew. Chem. Int. Ed.* **2022**, *61*, e202206680; k) S. Q. Moles, M. M. Haley, M. Kertesz, J. Casado, *Angew. Chem. Int. Ed.* **2022**, *61*, e202209138; l) W. Kueh, X. Shi, W. T. Phua, H. Kueh, C. Y. Liau, C. Chi, *Org. Lett.* **2022**, *24*, 5935–5940; m) K. Wang, Q. Zhan, B. Han, M. S. Quintero, W. Huang, Y. Ji, F. Miao, H. Chen, J. Casado, Y. Zheng, *J. Mater. Chem. C* **2022**, *10*, 12724–12730; n) P. Wang, J. Hu, Z. Xu, Z. Pu, S. Sato, X. Zhang, W. Hu, Z. Sun, *Chem. Commun.* **2023**, *59*, 2015–2018; o) X. Xu, S. Takebayashi, H. Hanayama, S. Vasylevskyi, T. Onishi, T. Ohto, H. Tada, A. Narita, *J. Am. Chem. Soc.* **2023**, *145*, 3891–3896; p) F. Miao, Y. Ji, B. Han, M. S. Quintero, H. Chen, G. Xue, L. Cai, J. Casado, Y. Zheng, *Chem. Sci.* **2023**, *14*, 2698–2705; q) J. Guo, Z. Li, X. Tian, T. Zhang, Y. Wang, C. Dou, *Angew. Chem. Int. Ed.* **2023**, *62*, e202217470; r) T. Maeda, T. Oka, D. Sakamaki, H. Fujiwara, N. Suzuki, S. Yagi, T. Konishi, K. Kamada, *Chem. Sci.* **2023**, *14*, 1978–1985.
- [3] a) Z. Sun, Q. Ye, C. Chi, J. Wu, *Chem. Soc. Rev.* **2012**, *41*, 7857–7889; b) H. Hwang, D. Khim, J. M. Yun, E. Jung, S. Y. Jang, Y. H. Jang, Y. Y. Noh, D. Y. Kim, *Adv. Funct. Mater.* **2015**, *25*, 1146–1156; c) D. Venkateshvaran, M. Nikolka, A. Sadhanala, V. Lemaur, M. Zelazny, M. Kepa, M. Hurhangie, A. J. Kronemeijer, V. Pecunia, I. Nasrallah, I. Romanov, K. Broch, I. McCulloch, D. Emin, Y. Olivier, J. Cornil, D. Beljonne, H. Sirringhaus, *Nature* **2014**, *515*, 384–388.
- [4] a) A. Rajca, *Chem. Rev.* **1994**, *94*, 871–893; b) A. Rajca, J. Wongsiriratanakul, S. Rajca, *Science* **2001**, *294*, 1503–1505; c) N. M. Gallagher, A. Olankitwanit, A. Rajca, *J. Org. Chem.* **2015**, *80*, 1291–1298; d) A. Rajca, S. Rajca, J. Wongsiriratanakul, *J. Am. Chem. Soc.* **1999**, *6308*–6309.
- [5] a) M. Abe, C. Ishihara, A. Tagegami, *J. Org. Chem.* **2004**, *69*, 7250–7255.
- [6] M. Abe, J. Ye, M. Mishima, *Chem. Soc. Rev.* **2012**, *41*, 3808–3820.
- [7] a) M. Abe, R. Akisaka, *Chem. Lett.* **2017**, 1586–1592; b) Z. Wang, R. Akisaka, S. Yabumoto, T. Nakagawa, S. Hatano, M. Abe, *Chem. Sci.* **2021**, *12*, 613–625.
- [8] Y. Miyazawa, Z. Wang, M. Matsumoto, S. Hatano, I. Antol, E. Kayahara, S. Yamago, M. Abe, *J. Am. Chem. Soc.* **2021**, *143*, 7426–7439.
- [9] R. Jasti, J. Bhattacharjee, J. B. Neaton, C. R. Bertozzi, *J. Am. Chem. Soc.* **2008**, *17646*–17647.
- [10] a) C. Lee, W. Yang, R. G. Parr, *Phys. Rev. B* **1988**, *37*, 785–789; b) A. D. Becke, *J. Chem. Phys.* **1993**, *98*, 5648–5652; c) R. Ditchfield, *Mol. Phys.* **1974**, *27*, 789–807; d) N. B. Er, R. Mcweeny, *Phys. Rev.* **1962**, *126*, 1028–1034; e) K. Wolinsky, J. F. Hinton, P. Pulay, *J. Am. Chem. Soc.* **1990**, *112*, 8251–8260.
- [11] R. E. Stratmann, G. E. Scuseria, M. J. Frisch, *J. Chem. Phys.* **1998**, *109*, 8218–8224.
- [12] Y. Zhao, D. G. Truhlar, *Theor. Chem. Acc.* **2008**, *120*, 215–241.
- [13] M. Abe, S. Watanabe, H. Tamura, S. Boinapally, K. Kanahara, Y. Fujiwara, *J. Org. Chem.* **2013**, *78*, 1940–1948.
- [14] I. Ahmd, S. Ahmed, M. A. Sheraz, M. Aminuddin, F. Hussain, M. Vaid, *Chem. Pharm. Bull.* **2009**, *57*, 1363–1370.
- [15] a) G. Prter, *Proc. R. Soc. Lond.* **1950**, *A200*, 284–300; b) R. G. W. Norrish, G. Porter, *Nature* **1949**, *164*, 658.

- [16] T. Nakagawa, K. Okamoto, H. Hanada, R. Katoh, *Opt. Lett.* **2016**, *41*, 1498–1501.
- [17] a) J. B. Fenn, M. Mann, C. K. Meng, S. F. Wong, C. M. Whitehouse, *Science* **1989**, *246*, 64–71; b) J. Zeleny, *Phys. Rev.* **1914**, *3*, 69–91.
- [18] W. Adam, W. Maas, W. M. Nau, *J. Org. Chem.* **2000**, *65*, 8790–8796.
- [19] a) S. L. Buchwalter, G. L. Closs, *J. Am. Chem. Soc.* **1975**, *97*, 3857–3858; b) S. L. Buchwalter, G. L. Closs, *J. Am. Chem. Soc.* **1979**, *101*, 4688–4694; c) M. P. Conrad, R. M. Pitzer, H. F. Schaefer III, *J. Am. Chem. Soc.* **1979**, *101*, 2245–2246; d) D. A. Dougherty, *Acc. Chem. Res.* **1991**, *24*, 88–94; e) W. Adam, H. M. Harrer, F. Kita, W. M. Nau, *Adv. Photochem.* **1998**, *24*, 205–254.
- [20] a) S. Sinnicker, F. Neese, *J. Phys. Chem. A* **2006**, *110*, 12267–12275; b) F. Neese, *J. Chem. Phys.* **2007**, *127*, 164112.
- [21] a) F. Neese, *Wiley Interdiscip. Rev. Comput. Mol. Sci.* **2012**, *2*, 73–78; b) F. Neese, *Wiley Interdiscip. Rev. Comput. Mol. Sci.* **2018**, *8*, 4–9.
- [22] H. Matsuoka, N. Ozawa, T. Kodama, H. Nishikawa, I. Ikemoto, K. Kikuchi, K. Furukawa, K. Sato, D. Shiomi, T. Takui, T. Kato, *J. Phys. Chem. B* **2004**, *108*, 13972–13976.
- [23] a) K. Sato, M. Yano, M. Furuichi, D. Shiomi, T. Takui, K. Abe, K. Itoh, A. Higuchi, K. Katsuma, Y. Shirota, *J. Am. Chem. Soc.* **1997**, *119*, 6607–6613; b) H. Matsuoka, K. Sato, D. Shiomi, T. Takui, *Appl. Magn. Reson.* **2003**, *23*, 517–538; c) A. V. Astashkin, A. Schweiger, *Chem. Phys. Lett.* **1990**, *174*, 595–602.
- [24] Y. Takahara, K. Yamaguchi, T. Fueno, *Chem. Phys. Lett.* **1989**, *157*, 211–216.
- [25] Y. Kitagawa, T. Saito, K. Yamaguchi, Approximate Spin Projection for Broken-Symmetry Method and Its Application. In *Symmetry (Group Theory) and Mathematical Treatment in Chemistry*, Editor: Akitsu, T., IntechOpen, **2018**, chapter 7.
- [26] a) K. Yamaguchi, T. Fljeno, *Chem. Phys. Lett.* **1989**, *159*, 465–471; b) Y. Kitagawa, T. Saito, M. Ito, M. Shoji, K. Koizumi, S. Yamanaka, T. Kawakami, M. Okumura, K. Yamaguchi, *Chem. Phys. Lett.* **2007**, *442*, 445–450; c) K. Yamaguchi, M. Okumura, W. Mori, J. Maki, K. Takada, T. Noro, *Chem. Phys. Lett.* **1993**, *210*, 201–210.
- [27] Y. Kitagawa, T. Saito, Y. Nakanishi, Y. Kataoka, T. Matsui, T. Kawakami, M. Okumura, K. Yamaguchi, *J. Phys. Chem. A* **2009**, *113*, 15041–15046.
- [28] B. Bleaney, K. D. Bowers, *Proc. R. Soc. A* **1952**, *43*, 372–374.

Manuscript received: March 29, 2023

Accepted manuscript online: May 3, 2023

Version of record online: June 16, 2023